

# Modes of Subwavelength Plasmonic Slot Waveguides

Georgios Veronis, *Member, IEEE*, and Shanhui Fan, *Senior Member, IEEE*

(Invited Paper)

**Abstract**—We investigate the properties of the modes that are supported by 3-D subwavelength plasmonic slot waveguides. We first show that the fundamental mode that is supported by a symmetric plasmonic slot waveguide, which is composed of a subwavelength slot in a thin metallic film embedded in an infinite homogeneous dielectric, is always a bound mode for any combination of operating wavelength and waveguide parameters. Its modal fields are highly confined over a wavelength range extending from zero frequency to the ultraviolet. We then show that for an asymmetric plasmonic slot waveguide, in which the surrounding dielectric media above and below the metal film are different, there may exist a cutoff slot width and/or a cutoff metal film thickness above which the mode becomes leaky, and there always exists a cutoff wavelength above which the mode becomes leaky. We investigate in detail the effect of variations of the parameters of the symmetric and asymmetric plasmonic slot waveguides. We also consider related alternative 3-D plasmonic waveguide geometries, such as a plasmonic slot waveguide, in which the two metal film regions that form the slot have a finite width, and a plasmonic strip waveguide, which is formed between a metallic strip and a metallic substrate. We show that for a specific modal size, the fundamental mode of the standard plasmonic slot waveguide has a larger propagation length compared with the corresponding modes of these plasmonic waveguides.

**Index Terms**—Integrated optics, optical waveguides, surface plasmons.

## I. INTRODUCTION

**G**UIDING electromagnetic waves with a mode at deep subwavelength scale has been of great interest recently. In the visible wavelength range, the typical way to create a subwavelength waveguide involves the use of so-called surface plasmon polaritons (SPPs). SPPs are bound nonradiative surface modes that propagate at metal–dielectric interfaces with field components that decay exponentially with distance away from the interface [1]. The decay length of the fields can be much smaller than the wavelength near the surface plasmon frequency. Several different plasmonic waveguiding structures have been proposed [2]–[8], such as metallic nanowires [3], [4], metallic nanoparticle arrays [5], [6], and V-shaped grooves

[7], [8]. However, such geometries are fundamentally limited by the fact that they support a highly confined mode *only* near the surface plasmon frequency. In this regime, the optical mode typically has low group velocity and short propagation length.

At microwave frequencies, where metals do not have a plasmonic response, two-conductor waveguides are used to guide subwavelength modes. Such waveguiding structures always support a fundamental transverse electromagnetic (TEM) or quasi-TEM mode, which can have a deep subwavelength size and a broad guiding bandwidth [9]. In addition, it has been shown that the guiding wavelength range of subwavelength modes by such structures extends into the infrared and visible wavelengths [10]. In the optical wavelength range, however, metals have a plasmonic response [11]. The properties of the optical modes that are supported by plasmonic two-conductor waveguides are, therefore, quite different from those of their counterparts at microwave frequencies, where metals behave almost as perfect electric conductors [9]. Several different plasmonic two-conductor waveguide structures have been proposed to guide light [12]–[17]. Because of the predicted attractive properties of the plasmonic two-conductor waveguides, people have also started to experimentally explore such structures [18], [19].

Among all the plasmonic two-conductor waveguides, a 3-D plasmonic waveguide based on a deep subwavelength slot in a thin metallic film was recently investigated [15]–[17]. The geometry of such a plasmonic slot waveguide is shown in Fig. 1(a). It consists of a slot in a thin metal film. The thin metal film is embedded in dielectric. The supported optical mode is highly localized in the slot, and its direction of propagation is parallel to the slot. Fig. 1(b) shows a cross-sectional view of the waveguide geometry. It was shown that such a plasmonic slot waveguide supports a fundamental bound mode with size almost completely dominated by the near field of the slot over a wide range of frequencies [15]. The size of this mode can be far smaller than the wavelength, even when its effective index approaches that of the substrate. In addition, the group velocity of the mode is close to the speed of light in the substrate, and its propagation length is tens of micrometers at the optical communication wavelength ( $\lambda_0 = 1.55 \mu\text{m}$ ). Thus, such a plasmonic slot waveguide could be potentially important in providing an interface between conventional optics and subwavelength electronic and optoelectronic devices. The characteristics of the modes that are supported by the plasmonic slot waveguides at visible wavelengths ( $\lambda_0 = 632.8 \text{ nm}$ ) have also been investigated [16], [17].

Manuscript received June 8, 2007. This work was supported in part by DARPA/MARCO under the Interconnect Focus Center and by the Air Force Office of Scientific Research under Grant FA 9550-04-1-0437.

The authors are with the Department of Electrical Engineering, Stanford University, Stanford, CA 94305 USA (e-mail: gveronis@stanford.edu; shanhui@stanford.edu).

Color versions of one or more of the figures in this paper are available online at <http://ieeexplore.ieee.org>.

Digital Object Identifier 10.1109/JLT.2007.903544

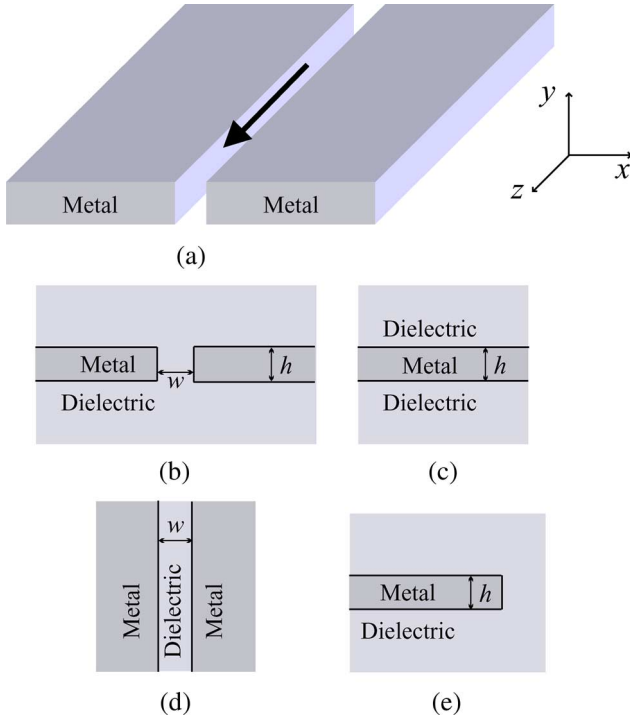


Fig. 1. (a) Geometry of a 3-D plasmonic slot waveguide. The arrow shows the direction of propagation of the optical mode. (b) Cross-sectional view of the 3-D plasmonic slot waveguide geometry. (c)–(e) Corresponding DMD, MDM, and truncated metal film structures for the 3-D plasmonic slot waveguide of (b).

In this paper, we investigate in detail the characteristics of the modes that are supported by 3-D plasmonic slot waveguides. In particular, we illustrate the physics of such a waveguide by comparing it to a number of simplified geometries shown in Fig. 1(c)–(e). We first consider a reference symmetric plasmonic slot waveguide structure, which is composed of a slot in a thin metallic film that is embedded in an infinite homogeneous dielectric. We show that the fundamental mode that is supported by this symmetric plasmonic slot waveguide is always a bound mode for any combination of operating wavelength and waveguide parameters. We then consider an asymmetric plasmonic slot waveguide structure in which the surrounding dielectric media above and below the metal film are different. Unlike in the symmetric case, in the asymmetric case, the fundamental propagating mode is not always bound. We show that for a specific asymmetric plasmonic slot waveguide, there may exist a cutoff slot width and/or a cutoff metal film thickness above which the mode becomes leaky, and there always exists a cutoff wavelength above which the mode becomes leaky. We also consider related alternative 3-D plasmonic waveguide geometries. More specifically, we investigate a plasmonic slot waveguide, where the two metal film regions that form the slot have a finite width, and a plasmonic strip waveguide, which is formed between a metallic strip and a metallic substrate. We show that for a specific modal size, the fundamental mode of the reference plasmonic slot waveguide has a larger propagation length compared with the corresponding modes of these plasmonic waveguides.

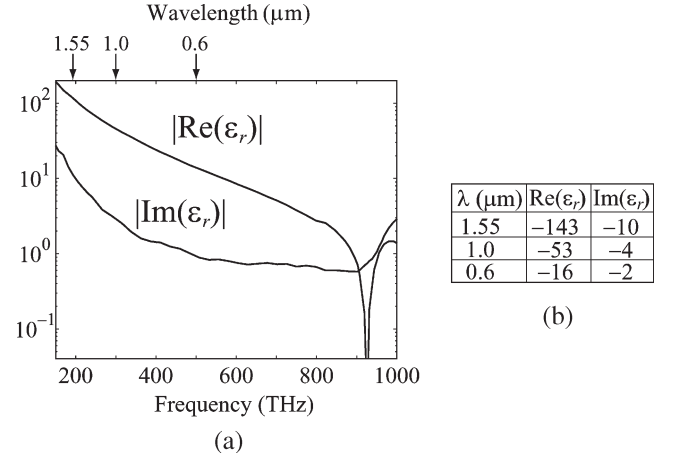


Fig. 2. (a) Absolute values of the real  $[\text{Re}(\epsilon_r)]$  and imaginary  $[\text{Im}(\epsilon_r)]$  part of the dielectric constant of silver at optical frequencies.  $\text{Re}(\epsilon_r) < 0$  for frequencies below  $\sim 910$  THz. (b) Dielectric constant of silver at selected wavelengths that are considered in this paper.

## II. SIMULATION METHOD

We calculate the eigenmodes of plasmonic waveguides at a given wavelength  $\lambda_0$  using a full-vectorial finite-difference frequency-domain (FDFD) mode solver [15], [20]. For waveguiding structures that are uniform in the  $z$  direction, if an  $\exp(-\gamma z)$  dependence is assumed for all field components, Maxwell's equations reduce to two coupled equations for the transverse magnetic field components  $H_x$  and  $H_y$  [20], i.e.,

$$\begin{aligned}
 -\epsilon_r k_0^2 h_x + \epsilon_r \frac{\partial}{\partial y} \left[ \epsilon_r^{-1} \left( \frac{\partial h_y}{\partial x} - \frac{\partial h_x}{\partial y} \right) \right] - \frac{\partial}{\partial x} \left( \frac{\partial h_x}{\partial x} + \frac{\partial h_y}{\partial y} \right) &= \gamma^2 h_x \\
 -\epsilon_r k_0^2 h_y - \epsilon_r \frac{\partial}{\partial x} \left[ \epsilon_r^{-1} \left( \frac{\partial h_y}{\partial x} - \frac{\partial h_x}{\partial y} \right) \right] - \frac{\partial}{\partial y} \left( \frac{\partial h_x}{\partial x} + \frac{\partial h_y}{\partial y} \right) &= \gamma^2 h_y
 \end{aligned}$$

where  $\mathbf{H}(x, y, z) = \mathbf{h}(x, y) \exp(-\gamma z)$ ,  $\epsilon_r = \epsilon_r(x, y)$  is the dielectric function, and  $k_0^2 = \omega^2 \epsilon_0 \mu_0$ . Solving these eigenvalue equations allows one to define the propagation length  $L_p$  and the effective index  $n_{\text{eff}}$  of a propagating mode through the equation  $\gamma \equiv L_p^{-1} + i\beta = L_p^{-1} + i2\pi n_{\text{eff}} \lambda_0^{-1}$ . Also, the dispersion relation is defined as  $\omega = \omega(\beta)$ . These equations are discretized on a nonuniform orthogonal grid that results in a sparse matrix eigenvalue problem of the form  $\mathbf{A}\mathbf{h} = \gamma^2 \mathbf{h}$ , which is solved using iterative sparse eigenvalue techniques [21]. The discretization scheme is based on Yee's lattice [20]. To calculate the bound eigenmodes of the waveguide, we ensure that the size of the computational domain is large enough so that the fields are negligibly small at its boundaries [22], whereas for leaky modes, we use perfectly matched layer absorbing boundary conditions [21]. An important feature of this formulation is the absence of spurious modes [22]. In addition, metals have complicated dispersion properties in the optical wavelength range. As an example, Fig. 2 shows the real and imaginary parts of the dielectric constant of silver at optical frequencies [11], [23]. The frequency-domain mode solver allows us to directly use experimental data for the frequency-dependent dielectric constant of metals, including both the real and imaginary parts, with no approximation.

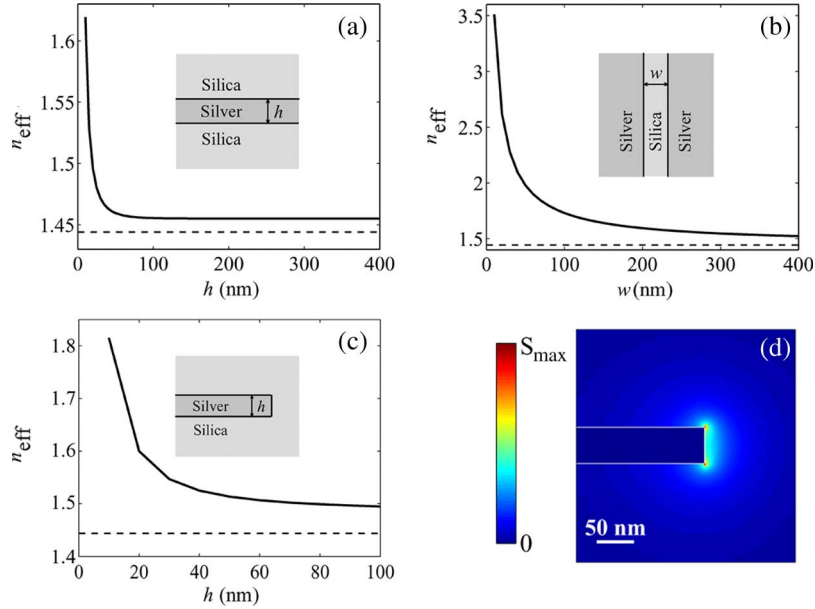


Fig. 3. (a) (Solid line) Effective index  $n_{\text{eff}}$  of the high-index mode of a silica–silver–silica DMD structure (see inset) as a function of the width of the central silver region  $h$ . (Dashed line) Refractive index of silica. (b) (Solid line) Effective index  $n_{\text{eff}}$  of the fundamental mode of a silver–silica–silver MDM structure (see inset) as a function of the width of the central silica region  $w$ . (Dashed line) Refractive index of silica. (c) (Solid line) Effective index  $n_{\text{eff}}$  of the fundamental edge mode of a truncated silver film embedded in silica as a function of the metal film thickness  $h$ . (Dashed line) Refractive index of silica. (d) Power density profile of the edge mode that is supported by a truncated silver film embedded in silica for  $h = 50$  nm at  $\lambda_0 = 1.55$   $\mu\text{m}$ .

### III. SIMPLIFIED PLASMONIC STRUCTURES

In order to understand the modal structure of the slot waveguide that is shown in Fig. 1(a) and (b), we first consider the modes in the corresponding simplified geometries that include 2-D dielectric–metal–dielectric [DMD, Fig. 1(c)] and metal–dielectric–metal [MDM, Fig. 1(d)] plasmonic waveguiding structures, as well as the edge on a truncated metal film [Fig. 1(e)]. The asymptotic behavior of many properties of 3-D plasmonic slot waveguides can be explained in terms of the properties of these simpler plasmonic structures. Below, we focus only on those modes in these simplified structures that are directly related to the fundamental modes of the slot.

The corresponding DMD plasmonic structure [Fig. 1(c)] has the same metal film thickness as the film in the slot waveguide [Fig. 1(b)]. Such a structure supports two modes below the surface plasmon frequency [10]. Of relevance here is the higher index mode that has a symmetric charge distribution. In Fig. 3(a), we show the effective index  $n_{\text{eff}}$  of the high-index mode of a silica–silver–silica DMD structure as a function of the width of the central silver region  $h$ . As a somewhat unusual feature, when  $h$  decreases, the fraction of the modal power in the metal increases, and  $n_{\text{eff}}$ , therefore, increases. In the opposite limit, as  $h \rightarrow \infty$ , the coupling between the surface plasmon modes of the two metal–dielectric interfaces vanishes, and  $n_{\text{eff}}$ , therefore, asymptotically approaches the effective index of the surface plasmon mode of a single metal–dielectric interface.

The corresponding MDM plasmonic structure [Fig. 1(d)] has a dielectric film thickness equal to the slot width [Fig. 1(b)]. Such a structure supports a fundamental mode below the surface plasmon frequency with antisymmetric charge distribution [10]. In Fig. 3(b), we show the effective index  $n_{\text{eff}}$  of the fundamental mode of a silver–silica–silver MDM structure as

a function of the width of the central silica region  $w$ . As  $w$  decreases, the fraction of the modal power in the metal increases, and  $n_{\text{eff}}$ , therefore, increases. In the opposite limit, as  $w \rightarrow \infty$ ,  $n_{\text{eff}}$  asymptotically approaches the effective index of the surface plasmon mode of a single metal–dielectric interface, as in the DMD structure. We also note that for a given width of the central region, the coupling of the single-interface surface plasmon modes is substantially stronger in the MDM case compared to the DMD case since in the former, the coupling occurs through dielectric, whereas in the latter, it occurs through metal.

The corresponding truncated metal film structure [Fig. 1(e)] has the same metal film thickness as the film in the slot waveguide [Fig. 1(b)]. Such a structure supports a fundamental edge mode. In Fig. 3(d), we show the power density ( $S_z = (1/2)\text{Re}[\mathbf{E} \times \mathbf{H}^* \cdot \hat{z}]$ ) profile of the edge mode in a truncated silver film embedded in silica. Large modal intensity is observed at the silver–silica interface at the edge of the metal film. More specifically, the modal power density is maximum at the two edge corners due to the singular behavior of the electric field near the sharp edges [24]. In Fig. 3(c), we show the effective index  $n_{\text{eff}}$  of the fundamental edge mode of a truncated silver film embedded in silica as a function of the metal film thickness  $h$  (solid line). Similar to the DMD structure,  $n_{\text{eff}}$  increases as  $h$  decreases. In the opposite limit, as  $h \rightarrow \infty$ ,  $n_{\text{eff}}$  asymptotically approaches the effective index of the mode of a single  $90^\circ$  corner, which is higher than the effective index of a single-interface surface plasmon mode [25].

### IV. SYMMETRIC PLASMONIC SLOT WAVEGUIDE

We now consider a symmetric plasmonic slot waveguide structure that is composed of a slot in a thin metallic film

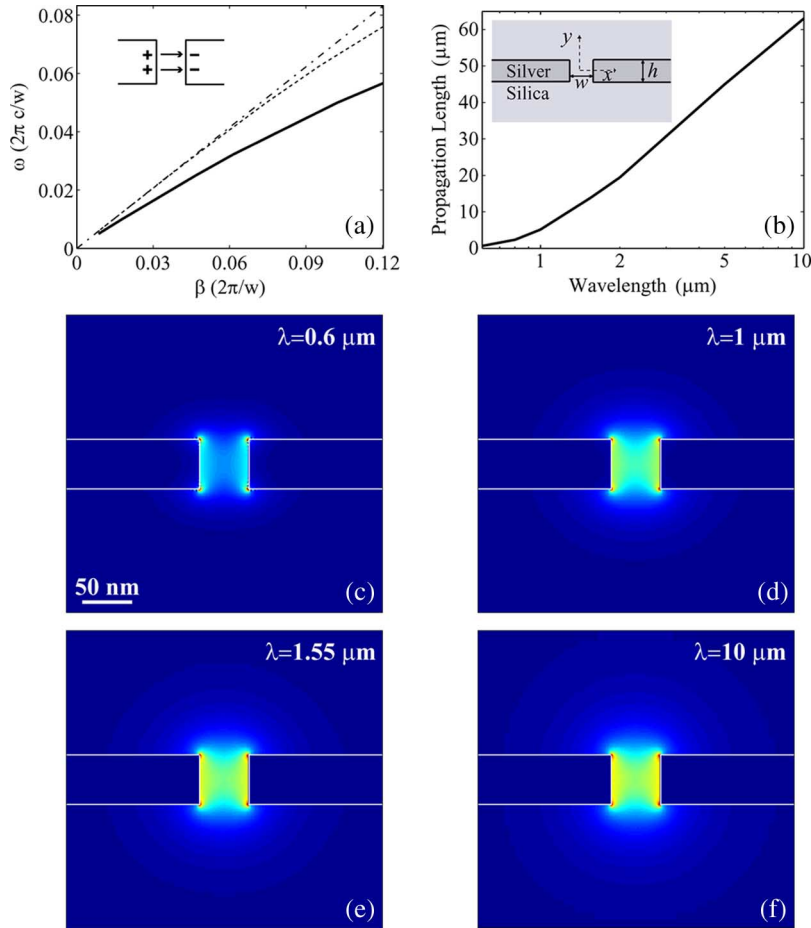


Fig. 4. (a) Dispersion relation of the fundamental mode of the symmetric plasmonic slot waveguide (shown with solid line) for  $w, h = 50 \text{ nm}$  [see inset of (b)]. The inset shows a schematic of the charge and vector field distribution of the mode. The dash-dotted line is the light line of silica, whereas the dashed curve is the dispersion relation of the higher index propagating mode in the silica–silver–silica thin film structure. (b) Propagation length of the fundamental mode of the symmetric plasmonic slot waveguide as a function of wavelength for  $w, h = 50 \text{ nm}$ . (c)–(f) Power density profile of the fundamental mode of the symmetric plasmonic slot waveguide for  $w, h = 50 \text{ nm}$  at  $\lambda_0 = 0.6, 1, 1.55, \text{ and } 10 \mu\text{m}$ .

embedded in an infinite homogeneous dielectric. We are particularly interested in the regime where the dimensions of the slot are much smaller than the wavelength of light. Thus, our reference structure consists of a slot of width  $w = 50 \text{ nm}$  in a silver film of thickness  $h = 50 \text{ nm}$  embedded in silica [ $n_s = 1.44$ ; inset of Fig. 4(b)].

In Fig. 4(a), we show the dispersion relation of the fundamental mode that is supported by our reference structure. We observe that the fundamental mode of the plasmonic slot waveguide has a wavevector that is larger than all the radiation modes in silica as well as all the propagating modes in the silica–silver–silica DMD thin film structure over the entire frequency range. The fundamental mode supported by our reference plasmonic slot waveguide is, therefore, a bound mode. Since the slot dimensions are much smaller than the wavelength in the frequency range of interest, this waveguide does not support any higher order propagating bound modes.

In Fig. 4(b), we show the propagation length  $L_p$  of the fundamental mode of our reference plasmonic slot waveguide as a function of wavelength. The propagation length decreases as the wavelength decreases. This is consistent with the behavior of plasmonic structures in general [1] since the fraction of the modal power in the metal increases at shorter wavelengths.

In Fig. 4(c)–(f), we show the power density profile of the fundamental mode that is supported by our reference structure at different wavelengths. The fundamental mode is quasi-TEM, with dominant field components  $E_x$  and  $H_y$  [15]. The charge distribution is, therefore, odd for the mirror plane that is normal to  $x$  and even for the mirror plane that is normal to  $y$  [inset of Fig. 4(a)]. We observe that over a wide wavelength range, the modal fields are highly confined in the slot region and only slightly extend in the adjacent silica regions above and below the slot. Thus, the modal size is almost completely dominated by the near field of the slot [15]. In addition, the size of this mode is far smaller than the wavelength even when its dispersion relation approaches the light line of the surrounding dielectric media [15]. This behavior is fundamentally different from that of conventional dielectric waveguides in which the mode significantly extends into the low-index cladding, as the dispersion relation of the optical mode approaches the cladding light line [26], [27]. It is also fundamentally different from that of single-metal plasmonic waveguides (e.g., V-shaped grooves) in which a deep subwavelength mode is obtained only in a limited wavelength range, where the modal dispersion relation is far from the light line of the surrounding dielectric [28].

Large modal intensity is observed at the silver–silica interfaces in the slot. Similar to the edge mode [Fig. 3(d)], the modal power density of a plasmonic slot waveguide reaches the maximum at the corners of the slot due to the singular behavior of the electric field near sharp edges [24]. However, we will show below that the characteristics of the mode do not strongly depend on the sharpness of the slot corners. At visible wavelengths ( $\lambda_0 = 600$  nm), the modal power is concentrated at the edges of the two semi-infinite metal film regions that form the slot, and the power density in the middle of the slot is small [Fig. 4(c)]. At this wavelength, the dielectric constant of silver is  $\epsilon_r \simeq -16 - 2i$  and has a relatively small magnitude (Fig. 2). Hence, the field strongly penetrates into the metal region. Also, since the fraction of the modal power in the metal is high enough, the edge mode of a truncated metal film [Fig. 1(e)] is tightly confined, with a decay length in the dielectric smaller than the slot width. At visible wavelengths, the fundamental mode of the plasmonic slot waveguide, therefore, is composed of the weakly coupled edge modes of the two semi-infinite metal film regions that form the slot [17]. Since the coupling is weak, the effective index of the fundamental mode is very close to the effective index of a single edge mode. Due to the large fraction of the modal power in the metal at  $\lambda_0 = 600$  nm ( $\omega = 0.083 \, 2\pi c/w$ ), the effective index of the mode  $n_{\text{eff}} = 2.45$  is much larger than the index of silica  $n_s$  [Fig. 4(a)], and its propagation length  $L_p = 0.6 \, \mu\text{m}$  is very short [Fig. 4(b)].

As the wavelength increases, the dielectric constant of metal increases in magnitude, the fraction of the modal power in the metal decreases, and, therefore, the effective index of the mode decreases, and its propagation length increases. For  $\lambda_0 = 1, 1.55,$  and  $10 \, \mu\text{m}$  ( $\omega = 0.05, 0.032, 0.005 \, 2\pi c/w$ ), the modal effective indexes are  $n_{\text{eff}} = 2.05, 1.91,$  and  $1.72$  [Fig. 4(a)], and the modal propagation length is  $L_p = 5, 14,$  and  $63 \, \mu\text{m}$  [Fig. 4(b)], respectively. In addition, at infrared wavelengths, the modal power density in the middle of the slot is significant [Fig. 4(d)–(f)]. Thus, at longer wavelengths, the mode can no longer be viewed as being composed of edge modes. In particular, the effective index of the fundamental mode of the slot is much larger than the effective index of the edge mode.

In the remainder of this section, we investigate the effect of variations of the parameters of our reference plasmonic slot waveguide structure on the modal characteristics. We focus on the optical communication wavelength ( $\lambda_0 = 1.55 \, \mu\text{m}$ ), where subwavelength plasmonic slot waveguides have propagation lengths of tens of micrometers [15].

In Fig. 5(a) and (b), we, respectively, show the effective index  $n_{\text{eff}}$  and the propagation length  $L_p$  of the fundamental mode of the plasmonic slot waveguide as a function of the slot width  $w$  [Fig. 4(b)]. All other parameters are as in our reference structure (Fig. 4). We observe that as  $w$  decreases,  $n_{\text{eff}}$  increases, and  $L_p$  decreases. This is due to the fact that as  $w$  decreases, the fraction of the modal power in the metal increases. A similar behavior is observed in MDM plasmonic waveguides [7], [12], [13]. In fact, for  $w \rightarrow 0$ , we observe that  $n_{\text{eff}}(w)$  is very close to  $n_{\text{eff}}(w)|_{\text{MDM}}$  [Fig. 5(a)]. In the limit of  $w \rightarrow \infty$ ,  $n_{\text{eff}}(w)$  asymptotically approaches the effective index of the edge mode [shown with the dash-dotted line in Fig. 5(a)], which is slightly higher than the effective index of

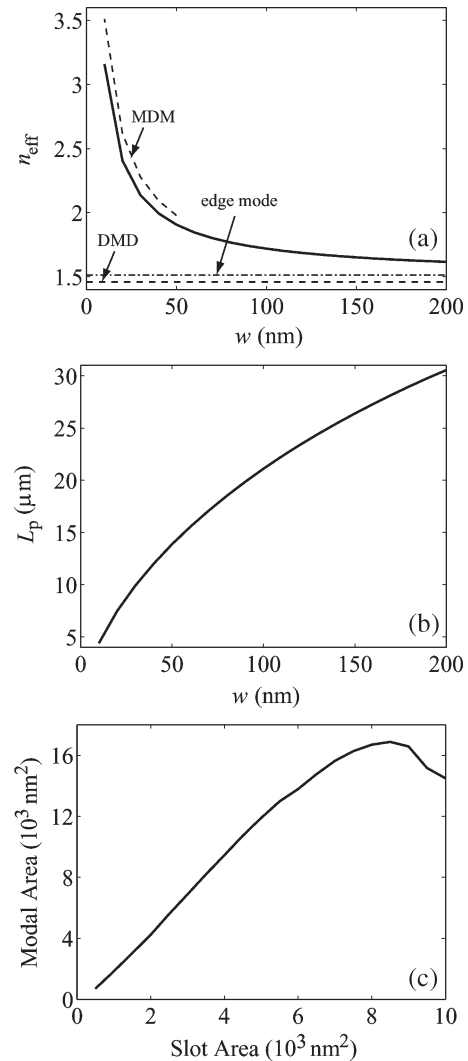


Fig. 5. (a) (Solid line) Effective index  $n_{\text{eff}}$  of the fundamental mode of the symmetric plasmonic slot waveguide as a function of the slot width  $w$  [Fig. 4(b)]. (Dashed line) Effective index of the fundamental mode of the corresponding MDM structure. (Dash-dotted line) Effective index of the high-index mode of the corresponding DMD structure. (Dashed line) Effective index of the edge mode of the corresponding truncated metallic film. (b) Propagation length  $L_p$  of the fundamental mode of the symmetric plasmonic slot waveguide as a function of the slot width  $w$  [Fig. 4(b)]. (c) Modal area of the fundamental mode of the symmetric plasmonic slot waveguide as a function of the slot area  $w \times h$ , as  $w$  is varied [Fig. 4(b)]. All other parameters are as in our reference structure (Fig. 4).

the high-index mode of the corresponding DMD structure [10] [shown with the dashed line in Fig. 5(a)]. The same asymptotic behaviors are also observed in the propagation length  $L_p(w)$  for  $w \rightarrow 0$  and  $w \rightarrow \infty$ . In Fig. 5(c), we show the modal area (defined as the area in which the mode power density is larger than  $1/e^2$  of its maximum value) of the fundamental mode of the plasmonic slot waveguide as a function of the slot area  $w \times h$ , as  $w$  is varied [Fig. 4(b)]. As expected, for small  $w$ , the modal area increases as  $w$  increases. In addition, the coupling between the edge modes of the two semi-infinite metal film regions that form the slot decreases as  $w$  increases. Therefore, when  $w$  is larger than the decay length of the edge mode in silica, the modal area decreases as  $w$  increases. As  $w \rightarrow \infty$ , the modal area asymptotically approaches twice the area of the edge mode.

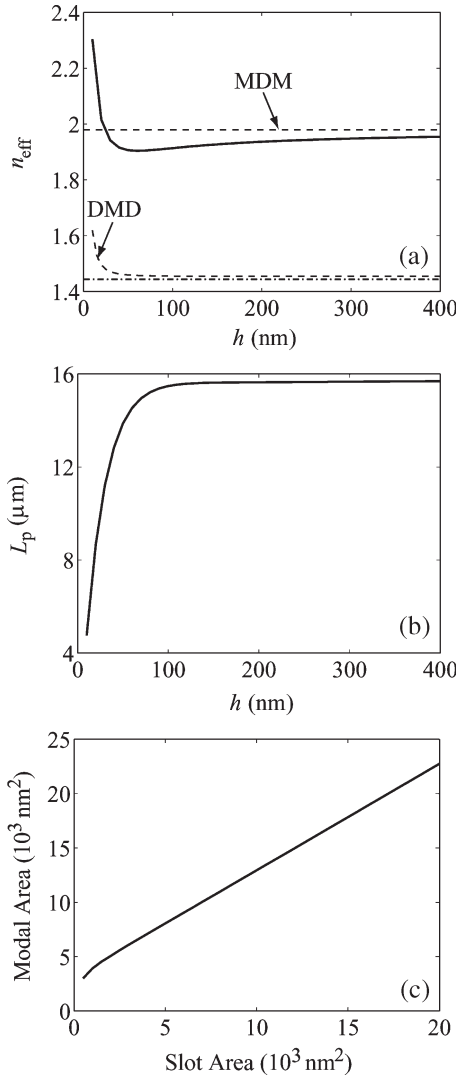


Fig. 6. (a) (Solid line) Effective index  $n_{\text{eff}}$  of the fundamental mode of the symmetric plasmonic slot waveguide as a function of the thickness  $h$  of the metallic film [Fig. 4(b)]. (Dashed line) Effective index of the fundamental mode of the corresponding MDM structure. (Dash-dotted line) Effective index of the high-index mode of the corresponding DMD structure. (Dash-dotted line) Refractive index of the substrate. (b) Propagation length  $L_p$  of the fundamental mode of the symmetric plasmonic slot waveguide as a function of the thickness  $h$  of the metallic film [Fig. 4(b)]. (c) Modal area of the fundamental mode of the symmetric plasmonic slot waveguide as a function of the slot area  $w \times h$ , as  $h$  is varied [Fig. 4(b)]. All other parameters are as in our reference structure (Fig. 4).

In Fig. 6(a) and (b), we, respectively, show the effective index  $n_{\text{eff}}$  and the propagation length  $L_p$  of the fundamental mode of the plasmonic slot waveguide as a function of the thickness  $h$  of the metallic film [Fig. 4(b)]. All other parameters are as in our reference structure (Fig. 4). As  $h \rightarrow \infty$ , the effective index of the mode asymptotically approaches the effective index of the fundamental mode of the corresponding MDM plasmonic waveguide [ $\lim_{h \rightarrow \infty} n_{\text{eff}}(h) = n_{\text{eff}}|_{\text{MDM}}$ ], and the same asymptotic behavior is observed in the propagation length  $L_p(h)$ . In Fig. 6(c), we show the modal area of the fundamental mode of the plasmonic slot waveguide as a function of the slot area  $w \times h$ , as  $h$  is varied [Fig. 4(b)]. The modal area increases as  $h$  increases, and for large  $h$ , the increase is linear.

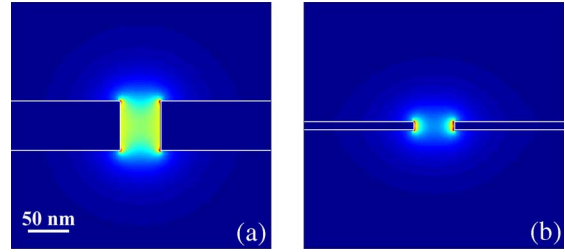


Fig. 7. (a) Power density profile of the fundamental mode of the symmetric plasmonic slot waveguide for  $w = 50 \text{ nm}$ , and  $h = 60 \text{ nm}$  at  $\lambda_0 = 1.55 \mu\text{m}$ . (b) Same as in (a), except  $h = 10 \text{ nm}$ .

We also observe that as  $h \rightarrow 0$ ,  $n_{\text{eff}}(h)$  increases, and  $L_p(h)$  decreases. We found that this behavior is related to the fringing fields of the mode rather than the fields in the slot region. The dominant components of the fringing fields are  $E_y$  and  $H_x$ , and they are maximum at the four lateral silver–silica interfaces at  $y = \pm h/2$ ,  $x > w/2$ , or  $x < -w/2$  [inset of Fig. 4(b)]. As the film thickness  $h$  decreases, the fraction of the modal power in the metal at these interfaces increases, and this results in an increasing effective index  $n_{\text{eff}}$  and a decreasing propagation length  $L_p$ . The same trend is also observed at visible wavelengths [17]. In Fig. 7(a) and (b), we show the power density profile of the fundamental mode of the plasmonic slot waveguide for  $h = 60 \text{ nm}$  and  $h = 10 \text{ nm}$ , respectively. All other parameters are as in our reference structure (Fig. 4). We observe that as the film thickness  $h$  decreases, the modal profile evolves into two weakly coupled edge modes. This is consistent with the increase of the effective index  $n_{\text{eff}}$ , which translates into smaller field decay length in dielectric, and also confirms that the effective index increase is related to the fringing fields of the mode at the semi-infinite metal film regions. We also observe that in the limit of  $h \rightarrow 0$ , the modal area approaches an asymptotic nonzero value [Fig. 6(c)], unlike the  $w \rightarrow 0$  case. In other words, there is a minimum modal size as the film thickness approaches zero due to the fringing fields of the mode.

We also investigated the effect of varying the dielectric constant of the medium in which the metallic film with the slot is embedded. We found that as the permittivity of the dielectric is increased, the effective index  $n_{\text{eff}}$  of the fundamental mode increases, and its propagation length  $L_p$  decreases. As in the case of a single-interface surface plasmon mode [1], this is due in part to increased fraction of the modal power in the metal, as the permittivity of the dielectric increases, as well as decreased group velocity. Finally, we note that in the case of the symmetric plasmonic slot waveguide, the wavevector of the fundamental mode is larger than all the radiation modes in the surrounding dielectric as well as all the propagating modes in the corresponding DMD thin film structure [Fig. 1(c)], for any combination of operating wavelength and waveguide parameters. In other words, in the symmetric plasmonic slot waveguide, there always exists a fundamental propagating bound mode, and there is no associated cutoff.

## V. ASYMMETRIC PLASMONIC SLOT WAVEGUIDE

We now consider an asymmetric plasmonic slot waveguide structure in which the surrounding dielectric media above

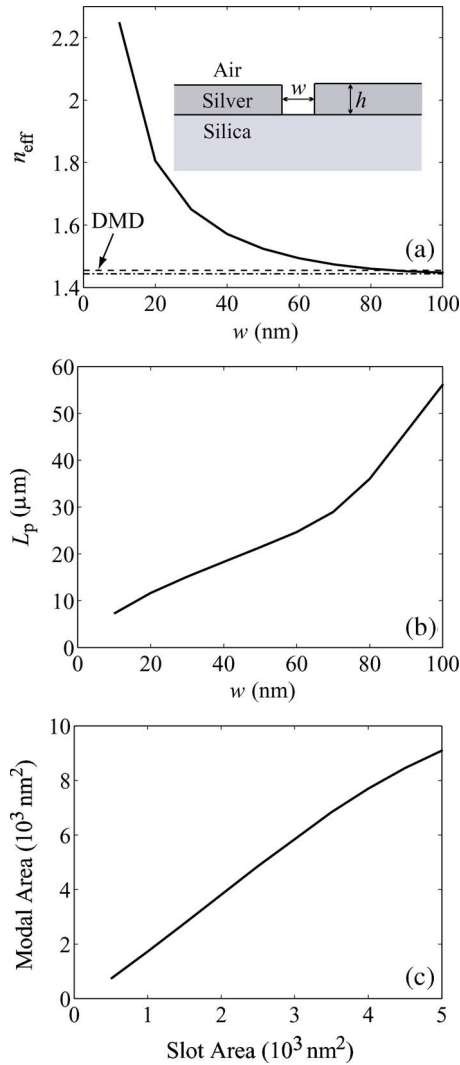


Fig. 8. (a) (Solid line) Effective index  $n_{\text{eff}}$  of the fundamental mode of the asymmetric plasmonic slot waveguide as a function of the slot width  $w$  (see inset). (Dashed line) Effective index of the high-index mode of the corresponding asymmetric DMD structure. (Dash-dotted line) Refractive index of the substrate. (b) Propagation length  $L_p$  of the fundamental mode of the asymmetric plasmonic slot waveguide as a function of the slot width  $w$  [Fig. 8(a)]. (c) Modal area of the fundamental mode of the asymmetric plasmonic slot waveguide as a function of the slot area  $w \times h$ , as  $w$  is varied [Fig. 8(a)]. All other parameters are as in our reference structure (Fig. 4).

and below the metal film are different. More specifically, we consider a waveguide that consists of an air slot of width  $w$  in a metallic film of thickness  $h$  deposited on silica [inset of Fig. 8(a)].

In Fig. 8(a) and (b), we, respectively, show the effective index  $n_{\text{eff}}$  and the propagation length  $L_p$  of the fundamental mode of the asymmetric plasmonic slot waveguide as a function of the slot width  $w$  [inset of Fig. 8(a)]. All other parameters are as in our reference structure (Fig. 4). In Fig. 8(c), we show the modal area of the fundamental mode of the asymmetric plasmonic slot waveguide as a function of the slot area  $w \times h$ , as  $w$  is varied. We observe that, in general, the effect of variation of the slot width  $w$  on the characteristics of the fundamental mode that is supported by the plasmonic slot waveguide is very similar in both the symmetric (Fig. 5) and asymmetric (Fig. 8)

cases. However, there is an important difference between the two cases with regard to the asymptotic behavior for  $w \rightarrow \infty$ . Unlike in the symmetric case, in the asymmetric case, the fundamental propagating mode is not always bound. If all other waveguide parameters are fixed, there is a slot width cutoff  $w_{\text{cutoff}}$ , and for  $w > w_{\text{cutoff}}$ , the mode is leaky. More specifically, we observe that if  $w$  is gradually increased to be  $w_{\text{cutoff}}$ , the modal power starts to leak into the propagating modes of the DMD air–silver–silica thin film structure, and if  $w$  is further increased so that  $w > w_{\text{cutoff, substrate}}$ , the modal power also leaks into the radiation modes in the silica substrate [Fig. 8(a)]. In general, as  $w \rightarrow \infty$ ,  $n_{\text{eff}}(w)$  asymptotically approaches the effective index of the edge mode of a truncated metal film that is deposited on the substrate. For the structure shown in the inset of Fig. 8(a), the effective index of the edge mode is smaller than the effective index of the high-index mode of the asymmetric DMD (air–silver–silica) structure. Hence, there exists a cutoff width  $w_{\text{cutoff}}$ . In addition, the effective index of the edge mode is also smaller than the refractive index of the substrate (silica in Fig. 8). Hence, there also exists a cutoff width  $w_{\text{cutoff, substrate}}$ . We also observe that the propagation length  $L_p$  of the fundamental mode of the asymmetric plasmonic slot waveguide increases with  $w$ , even when the mode becomes leaky. This indicates that the dominant loss mechanism is the material loss in the metal. As  $w$  increases, the mode becomes less confined, and the power loss in the metal decreases. Thus, although the radiation power loss increases with  $w$ , the overall power loss decreases. In fact, for  $w > w_{\text{cutoff}}$  in the asymmetric case [Fig. 8(b)], the propagation length  $L_p$  increases more rapidly with  $w$  compared to the symmetric case [Fig. 5(b)] because leakage further reduces the mode confinement and, therefore, the power loss in the metal.

In Fig. 9(a) and (b), we, respectively, show the effective index  $n_{\text{eff}}$  and the propagation length  $L_p$  of the fundamental mode of the asymmetric plasmonic slot waveguide as a function of the metallic film thickness  $h$  [inset of Fig. 8(a)]. All other parameters are as in our reference structure (Fig. 4). In Fig. 9(c), we show the modal area of the fundamental mode of the asymmetric plasmonic slot waveguide as a function of the slot area  $w \times h$ , as  $h$  is varied. As in the case of slot width  $w$  variation (Figs. 5 and 8), we observe that, in general, the effect of metallic film thickness  $h$  variation on the characteristics of the fundamental mode that is supported by the plasmonic slot waveguide is very similar in both the symmetric (Fig. 6) and asymmetric (Fig. 9) cases. The most important difference between the two cases is related to the asymptotic behavior for  $h \rightarrow \infty$ . In the asymmetric case, as  $h \rightarrow \infty$ , the effective index of the fundamental mode  $n_{\text{eff}}(h)$  asymptotically approaches the effective index of the mode of the MDM plasmonic waveguide, with dielectric core corresponding to the dielectric media in the slot. Since for the structure shown in Fig. 8 the effective index of the mode that is supported by this MDM structure (silver–air–silver in Fig. 8) is smaller than the effective index of the high-index mode of the asymmetric DMD structure (air–silver–silica in Fig. 8), there exists a cutoff film thickness  $h_{\text{cutoff}}$ . For  $h > h_{\text{cutoff}}$ , there is no longer a fundamental guided mode. In addition, for this structure, since the effective index of the MDM mode (silver–air–silver in Fig. 8) is smaller

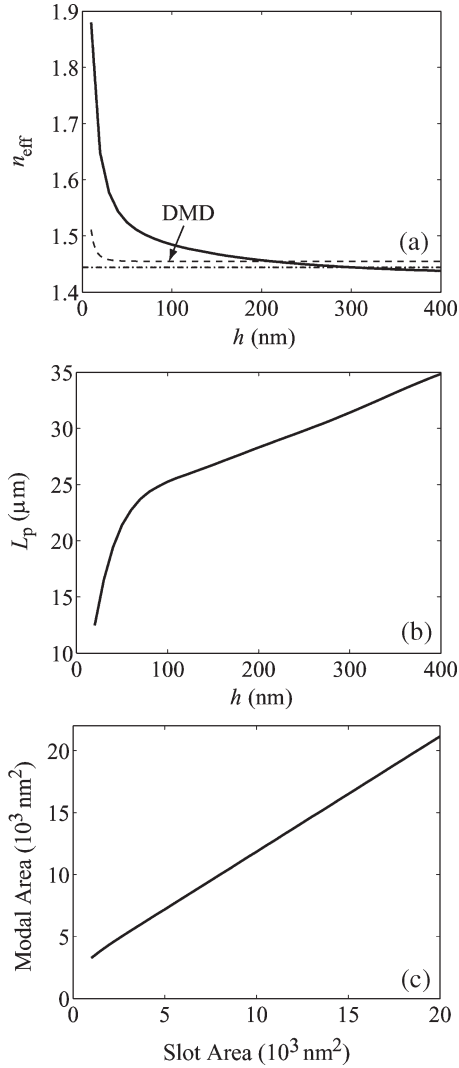


Fig. 9. (a) (Solid line) Effective index  $n_{\text{eff}}$  of the fundamental mode of the asymmetric plasmonic slot waveguide as a function of the thickness  $h$  of the metallic film [Fig. 8(a)]. (Dashed line) Effective index of the high-index mode of the corresponding asymmetric DMD structure. (Dash-dotted line) Refractive index of the substrate. (b) Propagation length  $L_p$  of the fundamental mode of the asymmetric plasmonic slot waveguide as a function of the thickness  $h$  of the metallic film [Fig. 8(a)]. (c) Modal area of the fundamental mode of the asymmetric plasmonic slot waveguide as a function of the slot area  $w \times h$ , as  $h$  is varied [Fig. 8(a)]. All other parameters are as in our reference structure (Fig. 4).

than the refractive index of the substrate (silica in Fig. 8), there also exists a cutoff film thickness due to the substrate  $h_{\text{cutoff, substrate}}$  above which the fundamental mode leaks into the substrate. We also observe that the propagation length  $L_p$  of the fundamental mode of the asymmetric plasmonic slot waveguide increases with  $h$ , even when the mode becomes leaky [Fig. 9(b)], for similar reasons as those mentioned above for the case of increasing  $w$ .

As mentioned above, the cutoff slot width depends on the effective index of the corresponding edge mode. Similarly, the cutoff film thickness depends on the effective index of the mode of the corresponding MDM plasmonic waveguide with dielectric core corresponding to the dielectric media in the slot. Therefore, the structure will not have a cutoff slot width or film thickness for the fundamental mode if the slot is filled with

the same dielectric as the substrate. We note, however, that for any asymmetric plasmonic slot waveguide, there always exists a cutoff wavelength above which the mode becomes leaky. This is due to the fact that in the long wavelength limit, metals behave as perfect electric conductors so that the modal fields do not penetrate into the metal. Since some of the field lines are in the upper and some are in the lower dielectric media, the effective index of the mode always lies between the refractive indexes of the upper and lower dielectric media, and the mode is, therefore, always leaky [15]. Finally, we note that as the structure becomes more asymmetric, the cutoff slot width, cutoff film thickness, and cutoff wavelength decrease.

## VI. EFFECT OF THE SHARPNESS OF THE SLOT CORNERS

In Fig. 10, we consider the effect of the sharpness of the slot corners on the characteristics of the fundamental mode that is supported by the plasmonic slot waveguide. More specifically, we consider the structure of (a), in which the corners of the two semi-infinite metal film regions are rounded with a radius  $0 < r_s < h/2$ . All other parameters are as in our reference structure (Fig. 4). We found that as  $r_s$  increases, the modal power density profile is modified, with the areas of high power density around the corners of the slot spreading out. In Fig. 10(b), we show the power density profile for the extreme case of  $r_s = h/2$ . In this case, we observe that unlike our reference slot structure, which has high power density areas around the upper and lower corners of the semi-infinite metal film regions, the mode exhibits high-density areas with maxima in the middle of the rounded edge of each of the metal film regions. In Fig. 10(c) and (d), we, respectively, show the effective index  $n_{\text{eff}}$  and the propagation length  $L_p$  of the fundamental mode of the plasmonic slot waveguide as a function of the radius  $r_s$  [Fig. 10(a)]. We observe that, despite the significant effect that  $r_s$  has on the modal power density profile, both  $n_{\text{eff}}$  and  $L_p$  are weakly dependent on  $r_s$ . Although the modal profile significantly changes, the fraction of the modal power in the metal does not change much. Thus, the basic characteristics of the fundamental mode that is supported by the plasmonic slot waveguide are *not* dependent on the sharpness of the slot corners. This observation implies that the performance of the slot waveguide is robust, in spite of the fact that the detailed shape of the sharp edges is difficult to control in the fabrication process.

## VII. RELATED ALTERNATIVE PLASMONIC WAVEGUIDES

We now consider related alternative 3-D plasmonic waveguides. In Fig. 11(a), we show a plasmonic slot waveguide in which the metal film regions that form the slot have a finite width  $w_{\text{strip}}$ . As above, we are interested in the regime where the dimensions of the slot  $w$  and  $h$ , as well as the strip width  $w_{\text{strip}}$ , are much smaller than the wavelength of light. For  $w_{\text{strip}} \rightarrow \infty$ , the modes that are supported by the waveguide of Fig. 11(a) asymptotically approach those of our reference plasmonic slot waveguide with semi-infinite metal film regions [Fig. 4(b)]. In order to understand the effect of a finite strip width, first, consider a single metal strip of width  $w_{\text{strip}}$  and

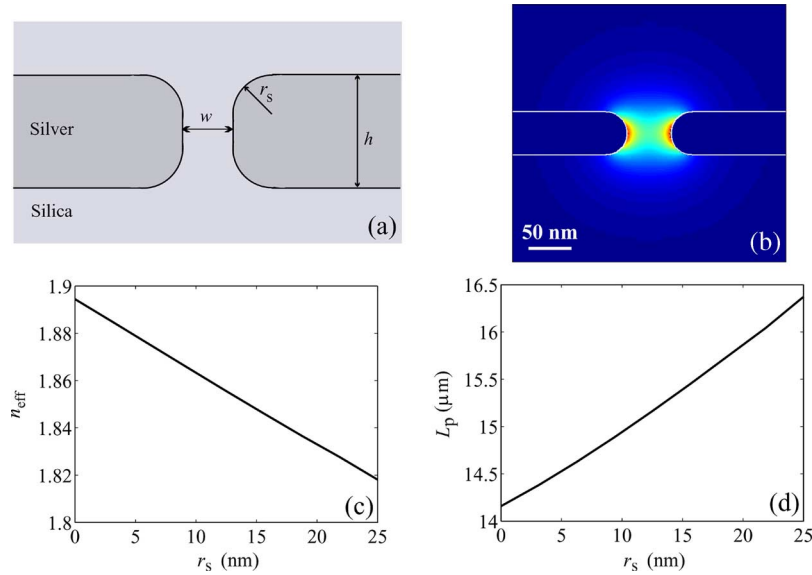


Fig. 10. (a) Schematic of a symmetric plasmonic slot waveguide, in which the corners of the two semi-infinite metal film regions are rounded with a radius  $0 < r_s < h/2$ . (b) Power density profile of the fundamental mode of the plasmonic slot waveguide of (a) for  $r_s = h/2$ . (c) Effective index  $n_{\text{eff}}$  of the fundamental mode of the plasmonic slot waveguide of (a) as a function of the radius  $r_s$ . (d) Propagation length  $L_p$  of the fundamental mode of the plasmonic slot waveguide of (a) as a function of the radius  $r_s$ . All other parameters are as in our reference structure (Fig. 4).

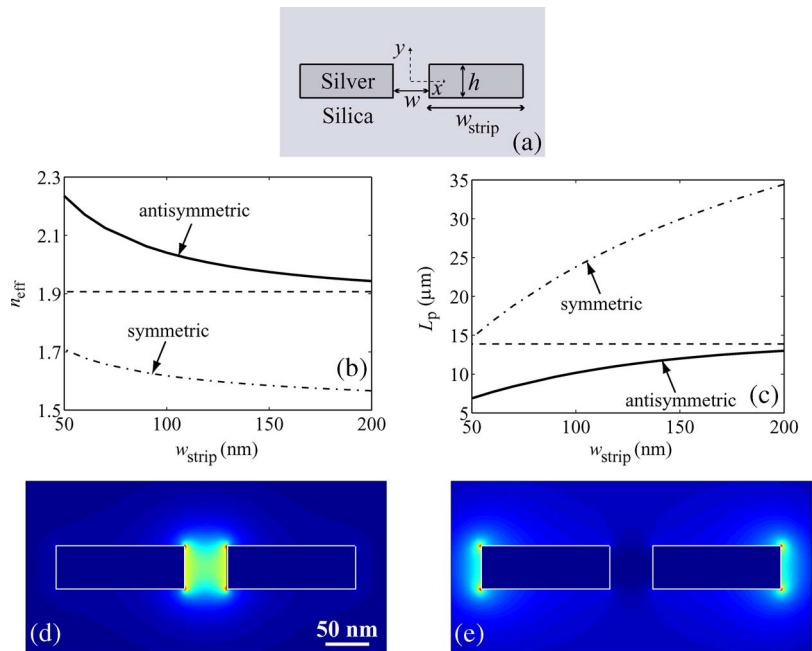


Fig. 11. (a) Schematic of a plasmonic slot waveguide, in which the two metal film regions that form the slot have a finite width  $w_{\text{strip}}$ . (b) Effective index  $n_{\text{eff}}$  of the (solid line) antisymmetric and (dash-dotted line) symmetric high-index modes of the plasmonic slot waveguide of (a) as a function of the metal strip width  $w_{\text{strip}}$ . (Dashed line) Effective index of the fundamental mode of our reference plasmonic slot waveguide [Fig. 4(b)]. (c) Propagation length  $L_p$  of the (solid line) antisymmetric and (dash-dotted line) symmetric high-index modes of the plasmonic slot waveguide of (a) as a function of the metal strip width  $w_{\text{strip}}$ . (Dashed line) Propagation length of the fundamental mode of our reference plasmonic slot waveguide [Fig. 4(b)]. All other parameters are as in our reference structure (Fig. 4). (d) Power density profile of the antisymmetric high-index mode of the plasmonic slot waveguide of (a) for  $w_{\text{strip}} = 200$  nm. (e) Power density profile of the symmetric high-index mode of the plasmonic slot waveguide of (a) for  $w_{\text{strip}} = 200$  nm. All other parameters are as in our reference structure (Fig. 4).

metal film thickness  $h$  embedded in an infinite homogeneous dielectric. When the metal strip dimensions are much smaller than the wavelength, the strip supports two distinct bound propagating modes. The first is a highly confined mode with maximum modal power density at the corners of the metal strip [29]. The second is a long-range surface plasmon mode [29], with effective index that is very close to the refractive index of

the surrounding dielectric and a very large modal area. When two such metal strips are brought in close proximity as in Fig. 11(a), their highly confined modes couple. The structure of Fig. 11(a), therefore, supports two bound propagating modes, which can be considered to result from the coupling of the highly confined single-strip modes. These two modes have their electric field distribution either symmetric or antisymmetric

with respect to the  $y$  axis. Note that an antisymmetric electric field distribution also implies an antisymmetric charge distribution [see, for example, the inset in Fig. 4(a)]. The power density profiles of the antisymmetric and symmetric modes are shown in Fig. 11(d) and (e), respectively. We observe that the modal profile of the antisymmetric mode [Fig. 11(d)] is very similar to the profile of the fundamental mode that is supported by our reference structure [Fig. 4(e)] with its modal fields highly confined in the slot region.

In Fig. 11(d) and (c), we, respectively, show the effective index  $n_{\text{eff}}$  and the propagation length  $L_p$  of the antisymmetric [Fig. 11(d)] and symmetric [Fig. 11(e)] modes of the plasmonic slot waveguide of Fig. 11(a) as a function of the metal strip width  $w_{\text{strip}}$ . All other parameters are as in our reference structure (Fig. 4). We also show with dashed line the effective index and the propagation length of the fundamental mode that is supported by our reference structure. We observe that the antisymmetric mode of the finite-width-film plasmonic slot waveguide [Fig. 11(a)], which is highly confined in the slot region, has a larger effective index and smaller propagation length than the fundamental mode of our reference plasmonic slot waveguide [inset of Fig. 4(b)]. As above, this is due to the fact that the fraction of the modal power in the metal is larger for the mode of Fig. 11(d) compared with the mode of Fig. 4(e). Similar behavior is also observed in 2-D plasmonic waveguides; the mode of a 2-D dielectric–metal–dielectric–metal–dielectric structure, which is highly confined in the central dielectric region, has a larger effective index and a smaller propagation length than the corresponding mode of an MDM structure with the same central dielectric region width [10]. We also observe that as  $w_{\text{strip}} \rightarrow \infty$ , the effective index of the antisymmetric mode of the finite-width-film plasmonic slot waveguide [Fig. 11(a)] asymptotically approaches the effective index of the fundamental mode of our reference plasmonic slot waveguide [inset of Fig. 4(b)], and the same asymptotic behavior is observed in the propagation length  $L_p(w_{\text{strip}})$ . Finally, we note that, in addition to the modes of Fig. 11, the finite-width-film plasmonic slot waveguide [Fig. 11(a)] supports long-range surface plasmon modes with effective indexes that are very close to the refractive index of the surrounding dielectric and, thus, smaller than those of the modes of Fig. 11.

We also considered a 3-D plasmonic strip waveguide [Fig. 12(a)], which is analogous to the microstrip waveguide used at microwave frequencies [9]. We found that the structure of Fig. 12(a) supports a highly confined mode in the region between the metal strip and the metallic substrate [Fig. 12(b)], with behavior very similar to that of the highly confined mode of the plasmonic slot waveguide with a finite film region [Fig. 11(a)]. In both cases, as  $w_{\text{strip}}$  decreases [Figs. 11(a) and 12(a)], the fraction of the modal power in the metal increases. Thus, for a specific modal size, the fundamental mode of the plasmonic strip waveguide [Fig. 12(a)] has a smaller propagation length compared to the fundamental mode of our reference plasmonic slot waveguide [inset of Fig. 4(b)]. We also found that the plasmonic strip waveguide [Fig. 12(a)] achieves similar performance to that of the plasmonic slot waveguide [inset of Fig. 4(b)] in terms of propagation length for a given modal size, only in the limit of  $w_{\text{strip}} \rightarrow \infty$ .

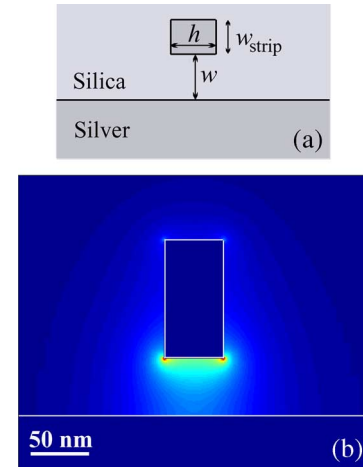


Fig. 12. (a) Schematic of a plasmonic strip waveguide, which is formed between a metallic strip and a metallic substrate. (b) Power density profile of the fundamental mode of the plasmonic strip waveguide for  $w = 50$  nm,  $h = 50$  nm, and  $w_{\text{strip}} = 100$  nm at  $\lambda_0 = 1.55$   $\mu\text{m}$ .

## VIII. SUMMARY

We investigated in detail the characteristics of the modes that are supported by 3-D subwavelength plasmonic slot waveguides. We calculated the eigenmodes of plasmonic waveguides at a given wavelength using a full-vectorial FDFD mode solver.

We first considered a reference symmetric plasmonic slot waveguide structure. The fundamental mode of this waveguide is always a bound mode for any combination of operating wavelength and waveguide parameters. Unlike single-metal plasmonic waveguides, its modal fields are highly confined over a wavelength range that extends from zero frequency to the ultraviolet.

We also investigated the effect of variations of the parameters of the symmetric slot waveguide on the characteristics of the supported modes. We found that, as the metallic film thickness approaches zero, the effective index of the fundamental mode increases, its propagation length decreases, and its modal area approaches an asymptotic nonzero value. This behavior is related to the fringing fields of the mode. We also found that the basic characteristics of the fundamental mode that is supported by the plasmonic slot waveguide are quite tolerant to variations on the sharpness of the slot corners that are associated with the fabrication process.

We then considered an asymmetric plasmonic slot waveguide structure in which the surrounding dielectric media above and below the metal film are different. Unlike in the symmetric case, in the asymmetric case, the fundamental propagating mode is not always bound. For a specific asymmetric plasmonic slot waveguide, there may exist a cutoff slot width and/or a cutoff metal film thickness above which the mode becomes leaky, and there always exists a cutoff wavelength above which the mode becomes leaky. We also found that when the fundamental mode of the asymmetric plasmonic waveguide becomes leaky, its propagation length is larger than the one of the symmetric plasmonic waveguide because leakage reduces the modal confinement and, therefore, the power loss in the metal.

We also considered related alternative 3-D plasmonic waveguide geometries. More specifically, we investigated the characteristics of the modes that are supported by a plasmonic slot waveguide, in which the two metal film regions that form the slot have a finite width, and by a plasmonic strip waveguide, which is formed between a metallic strip and a metallic substrate. We found that for a specific modal size, the fundamental mode of the reference plasmonic slot waveguide has a larger propagation length compared with the corresponding modes of these plasmonic waveguides.

#### ACKNOWLEDGMENT

The authors would like to acknowledge useful discussions with D. F. P. Pile, D. S. Ly-Gagnon, and M. L. Brongersma.

#### REFERENCES

- [1] W. L. Barnes, A. Dereux, and T. W. Ebbesen, "Surface plasmon subwavelength optics," *Nature*, vol. 424, no. 6950, pp. 824–830, Aug. 2003.
- [2] J. Takahara, S. Yamagishi, H. Taki, A. Morimoto, and T. Kobayashi, "Guiding of a one-dimensional optical beam with nanometer diameter," *Opt. Lett.*, vol. 22, no. 7, pp. 475–477, Apr. 1997.
- [3] J. C. Weeber, A. Dereux, C. Girard, J. R. Krenn, and J. P. Goudonnet, "Plasmon polaritons of metallic nanowires for controlling submicron propagation of light," *Phys. Rev. B, Condens. Matter*, vol. 60, no. 12, pp. 9061–9068, Sep. 1999.
- [4] J. R. Krenn, B. Lamprecht, H. Ditlbacher, G. Schider, M. Salerno, A. Leitner, and F. R. Aussenegg, "Non-diffraction-limited light transport by gold nanowires," *Europhys. Lett.*, vol. 60, no. 5, pp. 663–669, Dec. 2002.
- [5] M. L. Brongersma, J. W. Hartman, and H. A. Atwater, "Electromagnetic energy transfer and switching in nanoparticle chain arrays below the diffraction limit," *Phys. Rev. B, Condens. Matter*, vol. 62, no. 24, pp. R16 356–R16 359, Dec. 2000.
- [6] S. A. Maier, P. G. Kik, H. A. Atwater, S. Meltzer, E. Harel, B. E. Koel, and A. A. G. Requicha, "Local detection of electromagnetic energy transport below the diffraction limit in metal nanoparticle plasmon waveguides," *Nat. Mater.*, vol. 2, no. 4, pp. 229–232, Apr. 2003.
- [7] S. I. Bozhevolnyi, V. S. Volkov, E. Devaux, and T. W. Ebbesen, "Channel plasmon-polariton guiding by subwavelength metal grooves," *Phys. Rev. Lett.*, vol. 95, no. 4, p. 046 802, Jul. 2005.
- [8] S. I. Bozhevolnyi, V. S. Volkov, E. Devaux, J. Y. Laluet, and T. W. Ebbesen, "Channel plasmon subwavelength waveguide components including interferometers and ring resonators," *Nature*, vol. 440, no. 7083, pp. 508–511, Mar. 2006.
- [9] D. M. Pozar, *Microwave Engineering*. New York: Wiley, 1998.
- [10] E. N. Economou, "Surface plasmons in thin films," *Phys. Rev.*, vol. 182, no. 2, pp. 539–554, Jun. 1969.
- [11] E. D. Palik, *Handbook of Optical Constants of Solids*. New York: Academic, 1985.
- [12] R. Zia, M. D. Selker, P. B. Catrysse, and M. L. Brongersma, "Geometries and materials for subwavelength surface plasmon modes," *J. Opt. Soc. Amer. A, Opt. Image Sci.*, vol. 21, no. 12, pp. 2442–2446, Dec. 2004.
- [13] K. Tanaka and M. Tanaka, "Simulations of nanometric optical circuits based on surface plasmon polariton gap waveguide," *Appl. Phys. Lett.*, vol. 82, no. 8, pp. 1158–1160, Feb. 2003.
- [14] F. Kusunoki, T. Yotsuya, J. Takahara, and T. Kobayashi, "Propagation properties of guided waves in index-guided two-dimensional optical waveguides," *Appl. Phys. Lett.*, vol. 86, no. 21, p. 211 101, May 2005.
- [15] G. Veronis and S. Fan, "Guided subwavelength plasmonic mode supported by a slot in a thin metal film," *Opt. Lett.*, vol. 30, no. 24, pp. 3359–3361, Dec. 2005.
- [16] L. Liu, Z. Han, and S. He, "Novel surface plasmon waveguide for high integration," *Opt. Express*, vol. 13, no. 17, pp. 6645–6650, Aug. 2005.
- [17] D. F. P. Pile, T. Ogawa, D. K. Gramotnev, Y. Matsuzaki, K. C. Vernon, K. Yamaguchi, T. Okamoto, M. Haraguchi, and M. Fukui, "Two-dimensionally localized modes of a nanoscale gap plasmon waveguide," *Appl. Phys. Lett.*, vol. 87, no. 26, p. 261 114, Dec. 2005.
- [18] J. A. Dionne, H. J. Lezec, and H. A. Atwater, "Highly confined photon transport in subwavelength metallic slot waveguides," *Nano Lett.*, vol. 6, no. 9, pp. 1928–1932, Sep. 2006.
- [19] L. Chen, J. Shakya, and M. Lipson, "Subwavelength confinement in an integrated metal slot waveguide on silicon," *Opt. Lett.*, vol. 31, no. 14, pp. 2133–2135, Jul. 2006.
- [20] J. A. Pereda, A. Vegas, and A. Prieto, "An improved compact 2D full-wave FDFD method for general guided wave structures," *Microw. Opt. Technol. Lett.*, vol. 38, no. 4, pp. 331–335, Aug. 2003.
- [21] J. Jin, *The Finite Element Method in Electromagnetics*. New York: Wiley, 2002.
- [22] S. J. Al-Bader, "Optical transmission on metallic wires—Fundamental modes," *IEEE J. Quantum Electron.*, vol. 40, no. 3, pp. 325–329, Mar. 2004.
- [23] H. J. Hagemann, W. Gudat, and C. Kunz, "Optical constants from the far infrared to the X-ray region: Mg, Al, Cu, Ag, Au, Bi, C, and Al<sub>2</sub>O<sub>3</sub>," *J. Opt. Soc. Amer.*, vol. 65, no. 6, pp. 742–744, Jun. 1975.
- [24] J. D. Jackson, *Classical Electrodynamics*. New York: Wiley, 1999.
- [25] D. F. P. Pile, T. Ogawa, D. K. Gramotnev, T. Okamoto, M. Haraguchi, M. Fukui, and S. Matsuo, "Theoretical and experimental investigation of strongly localized plasmons on triangular metal wedges for subwavelength waveguiding," *Appl. Phys. Lett.*, vol. 87, no. 6, p. 061 106, Aug. 2005.
- [26] L. Vivien, S. Laval, E. Cassan, X. Le Roux, and D. Pascal, "2-D taper for low-loss coupling between polarization-insensitive microwaveguides and single-mode optical fibers," *J. Lightw. Technol.*, vol. 21, no. 10, pp. 2429–2433, Oct. 2003.
- [27] S. L. Chuang, *Physics of Optoelectronic Devices*. New York: Wiley, 1995.
- [28] E. Moreno, F. J. Garcia-Vidal, S. G. Rodrigo, L. Martin-Moreno, and S. I. Bozhevolnyi, "Channel plasmon-polaritons: Modal shape, dispersion, and losses," *Opt. Lett.*, vol. 31, no. 23, pp. 3447–3449, Dec. 2006.
- [29] P. Berini, "Plasmon-polariton waves guided by thin lossy metal films of finite width: Bound modes of symmetric structures," *Phys. Rev. B, Condens. Matter*, vol. 61, no. 15, pp. 10 484–10 503, Apr. 2000.



**Georgios Veronis** (M'99) received the B.S. degree in electrical engineering from the National Technical University of Athens, Athens, Greece, in 1997 and the M.S. and Ph.D. degrees in electrical engineering from Stanford University, Stanford, CA, in 1999 and 2002, respectively.

He is currently an Engineering Research Associate at Stanford University. He has published more than 20 refereed journal papers. His research interests include the theoretical analysis of nanophotonic and plasmonic devices and computational electromagnetics.



**Shanhui Fan** (M'05–SM'06) received the Ph.D. degree in theoretical condensed matter physics from the Massachusetts Institute of Technology (MIT), Cambridge, in 1997.

He is an Assistant Professor of electrical engineering at Stanford University, Stanford, CA. He was a Research Scientist at the Research Laboratory of Electronics, MIT, prior to his appointment at Stanford. He has published over 130 refereed journal articles, has given over 90 invited talks, and is the holder of 28 U.S. patents. His research interests are

in computational and theoretical studies of solid-state and photonic structures and devices, particularly photonic crystals, microcavities, and nanophotonic circuits and elements.

Dr. Fan is a member of the American Physical Society, the Optical Society of America, and the Society of Photo-Optical Instrumentation Engineers. He was a recipient of the National Science Foundation Career Award in 2002, a David and Lucile Packard Fellowship in Science and Engineering in 2003, and the National Academy of Sciences Award for Initiative in Research and the Adolph Lomb Medal from the Optical Society of America in 2007.